

Effect of Heating Rate on the Non-Isothermal Hydrogen Reduction of Hematite Pellets

Julia Brännberg FOGELSTRÖM  and Johan MARTINSSON* 

Business Area Metallurgy, Swerim AB, Isafjordsgatan 28A, 164 40 Kista, Sweden.

(Received September 18, 2024; Accepted December 4, 2024; Advance online published December 16, 2024; Published February 15, 2025)

Depending on the operational conditions inside a direct reduction shaft furnace, *e.g.*, ingoing gas temperature, feeding rate of material, and gas composition, the outgoing material will differ. This study investigates how the heating rate affects the reduction during pure hydrogen reduction of commercial iron ore pellets. As expected, the reduction rate increased with increasing heating rate. The heating rate also significantly affected the microstructure evolution inside the pellet. Inside the hydrogen direct reduced pellets, the iron had two appearances: (1) porous iron containing small and numerous intragranular pores, or (2) dense iron with larger but fewer intragranular pores. The pellet reduced with the slowest heating rate consisted of only porous iron, while the faster heating rates comprised porous and dense iron. The amount of dense iron gradually increased with increasing heating rate and was found to start forming at a temperature of around 668°C. The solid iron aggravated the mass transfer through the product layer and decreased the total reaction rate. This led to an expanded spread of the reaction zone as the heating rate increased. Through this work, it was also shown that insignificant reduction took place below a temperature of 450°C. Lastly, the microstructure that evolved during the non-isothermal reduction vastly differs from the microstructure formed during isothermal reduction. Consequently, an effective diffusivity and thermal conductivity that varies with time and temperature must be considered when optimizing the shaft furnace reactor.

KEY WORDS: non-isothermal reduction; hydrogen reduction; iron ore pellet; reduction mechanisms; microstructure.

1. Introduction

To combat the climate crisis, steel producers worldwide have initiated numerous projects to develop processes that emit less CO₂. Many projects involve the employment of direct reduction shaft furnaces, which use hydrogen as a reductant instead of natural gas, generating water as off-gas instead of CO₂.

In the direct reduced iron route, hematite pellets can be used as a burden. They are charged cold from the top of the reactor, and heated gas is introduced from the bottom. A counter-current flow of reaction gas and pellets takes place inside the reactor. The pellets will thereby experience non-isothermal conditions during reduction.

Although large-scale reduction shaft furnaces have been employed for several decades, operating them using pure hydrogen gas has only been tested on laboratory and pilot scales.¹⁾ The mechanisms of reduction are well established and are known as (1) mass transfer in the gas phase, (2)

mass transfer through the product layer, and (3) chemical reaction at the product/iron oxide interface. Studies often use resistances 1–3 to describe the rate-determining reduction steps. However, Hessling *et al.* showed the importance of considering heat transfer, especially for hydrogen reduction, since it is an endothermic reaction. Heat transfer was proven to be one limiting mechanism during isothermal hydrogen reduction of hematite pellets. It was found to partially limit the rate of reduction over a large reduction extent interval and, most profoundly, between the reduction extent of 20 to 40%.²⁾

Many researchers have studied the effect of temperature.^{3–7)} It has been shown that reducing iron oxide at higher temperatures generates a solid iron shell surrounding iron oxide grains, while when reducing at lower temperatures, a porous iron product is instead formed around the iron oxide grains. The diffusion rate inside the grains will vary depending on the formed microstructure, affecting the continued reduction.^{8–12)} The effect of temperature is hence essential to understand. Most of the studies have been conducted under isothermal conditions, and only a few studies have system-

* Corresponding author: E-mail: johan.martinsson@swerim.se



atically examined the effect of non-isothermal heating on the hydrogen reduction of iron oxide pellets.

Shimokawabe *et al.* studied the non-isothermal reduction of α -Fe₂O₃ powders prepared by different methods. The non-isothermal reduction experiments were conducted from room temperature to 800°C using a heating rate of 5°C/min under H₂-N₂ atmospheres. They found that powders prepared at 500 or 700°C went through a stepwise reduction. First, all Fe₂O₃ was reduced to Fe₃O₄ at approximately 11% reduction. Secondly, the Fe₃O₄ was either reduced directly to Fe or via FeO, depending on whether the reduction occurred below or above the wüstite temperature. The powders prepared at 900 or 1 200°C, on the other hand, did not show a stepwise reduction; instead, all reduction reactions occurred simultaneously.¹³⁾

Towhidi compared isothermal reduction to non-isothermal reduction under pure H₂ and H₂/CO atmosphere, under varying heating rates, *i.e.*, 2.5, 5, 7 and 10°C/min. The results showed that the overall rate of reduction for a non-isothermal reduction is slower than the isothermal reduction. Towhidi reported that the reduction rate reached a maximum at 5°C/min, after which the rate started to decrease again.¹⁴⁾

Hammam *et al.* studied the non-isothermal reduction of iron ore compacts in pure hydrogen from room temperature to 1 000°C, increasing the temperature with 5, 10, 15 and 20°C/min. It was found that no reduction occurred below 400°C and that the heating rate greatly affected the reduction rate and the structure of the iron grains.¹⁵⁾

Wright performed non-isothermal reductions of laboratory-made pellets using an H₂-CO-CO₂ reduction gas mixture, focusing on the volume change. It was found that the size of pores increased progressively from the pellet surface to the center. Wright also reported that the fine porous microstructure, formed at the surface of the pellet at low temperatures, coalesced by sintering at higher temperatures.¹²⁾

To the present authors' knowledge, no previous study has conducted a systematic study where the experiments have been terminated at elevated reduction degrees to evaluate the progress of non-isothermal reduction. The present work aims to increase the understanding of how different heating rates influence the reduction of iron ore pellets during non-isothermal reducing conditions using pure hydrogen gas, with a focus on both the reduction rate and the microstructural evolution. Based on the literature, this study's starting temperature of 450°C is relevant to the process.^{16–18)} On the other hand, the heating rate extends beyond the operating window of the shaft furnace process to provide more insights for the process optimization. Furthermore, the reduction mechanisms are evaluated and discussed with the help of scanning electron microscope (SEM) micrographs.

2. Experimental

2.1. Setup

A schematic illustration of the experimental setup is found in Fig. 1. The furnace is resistance-heated with FeCrAl heating elements and has a 5 cm homogenous high-temperature hot zone. A fused silica tube with an inner diameter of 40 mm, acting as a reaction chamber, is sealed from the surrounding atmosphere by O-rings at both ends. The O-rings are thermally protected by water-cooled

chambers. A gas inlet connected to the bottom leads into the reaction chamber, while a gas outlet is connected to the cooling chamber placed on top of the furnace.

A balance of model Ohaus Explorer EX2202/E (accuracy 0.01 g) is placed in an O-ring sealed box above the furnace, attached to a linear motion system to enable vertical movement. A steel tube is connected to the sealed box, and inside the steel tube, a small basket made of Nr-Cr wire, a total of 2.9 g, is hanging from the balance. The connection between the steel tube and the cooling chamber is gas-tight using a radial lip seal. To follow the experimental temperature, one Type K thermocouple is placed beside the basket, and another is placed inside the hot zone of the reaction chamber. Bronkhorst EL-FLOW select flow meters are used to set and control the gas composition and the flow rate.

2.2. Procedure

Commercial hematite pellets sourced from LKAB are used in this study. Table 1 shows the chemical composition and physical characteristics of the commercial pellets.¹⁹⁾ During each experiment, three pellets are used to minimize the effect of compositional variations in the commercial product. A previous study in this research group has shown that a total flow rate of hydrogen of 4 nL/min is enough to ensure that gas starvation does not limit the rate of isothermal reduction.²⁰⁾ As mentioned in the introduction, the non-isothermal reduction rate is slower than the isothermal reduction. Hence, the same flow rate was used in this study to eliminate the effect of gas starvation. Additionally, before any reduction, three inert pellets (Al₂O₃) with the same size as the commercial hematite pellets were used to calibrate the balance for the non-isothermal reductions. The calibration used the same method as when the hematite pellets were

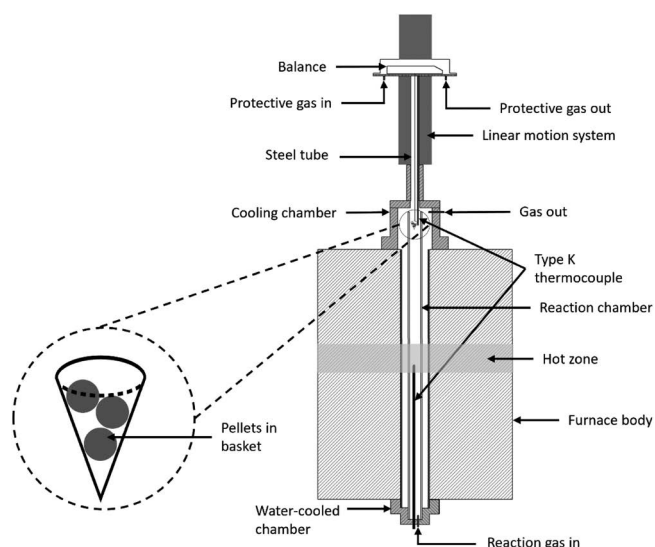


Fig. 1. Schematic illustration of the vertical tube furnace setup.

Table 1. Chemical composition and physical characteristics of commercial hematite pellets.

Fe ₂ O ₃	CaO	SiO ₂	MgO	Other	Porosity	Size
96.6 wt%	0.90 wt%	0.80 wt%	0.65 wt%	1.01 wt%	27%	10–12 mm

reduced.

The three hematite pellets were placed in the basket positioned in the cooling chamber. See Fig. 1 for the arrangement of the pellets. The lid to the furnace was closed, and the system was checked for vacuum to ensure a protective atmosphere. The atmosphere inside the furnace was evacuated and replaced with inert nitrogen gas (99.999%) multiple times. Then, the furnace was heated to 450°C while a 4 nL/min nitrogen flow rate was applied through the reaction chamber. After the furnace was hot, it was left to equilibrate for one hour. Using the linear motion system, the pellets were moved to the hot zone and left to acquire the temperature of 450°C. The reduction was initiated by introducing hydrogen gas (99.995%) into the reaction chamber with a flow rate of 4 nL/min. At the same time, the furnace was heated to 900°C using four different heating rates, namely, 7.7, 3.8, 2.5, and 1.9°C/min, respectively. The temperature was monitored, and the weight loss was recorded during the reduction experiment.

In addition, one reduction experiment was conducted to study the effect of subsequent heating at 900°C after non-isothermal reduction. The same procedure as for the non-isothermal reduction experiment conducted between 450 and 900°C, with a heating rate of 7.7°C/min, was used, with subsequent heating for one hour at 900°C.

While the focus of the work was the non-isothermal reduction, additional isothermal reduction experiments were conducted to deepen the understanding and aid the discussion. The pellets were kept inside the cooling chamber as the furnace was heated to 600°C or 900°C for the isothermal reduction experiments. At the same time, hydrogen with a flow rate of 4 nL/min was passing through the reaction chamber, setting the conditions for the experiment. After one hour of equilibration, the reduction was initiated by moving the pellets into the hot zone of the furnace. The weight loss was recorded during the reduction experiments.

Several experiments were terminated before complete reduction, at predetermined reduction extents, to study the evolution of the microstructure during the reduction using different heating rates. The pellets were moved rapidly to the cooling chamber to terminate the reductions, followed by flushing the furnace with nitrogen gas to remove the hydrogen gas. The microstructures were studied using scanning electron microscopy (SEM) of model ZEISS Sigma 300 VP, equipped with SE, BSE, and EDS detectors. For all experiments, a small flow rate of argon gas (99.999%) was kept inside the balance box throughout the experiment to prevent any generated water from coming into contact with the balance.

3. Results

Commercial iron ore pellets were reduced either isothermally or non-isothermally using pure hydrogen gas. Three pellets were reduced in every experiment to minimize the effect of compositional variations inside the commercial product. The results from the reduction experiments are presented as reduction extent, defined in Eq. (1):

$$R = \frac{w_0 - w_t}{w_0 - w_\infty} * 100\% \dots\dots\dots (1)$$

where w_0 is the initial weight of the pellets, w_t is the weight of the pellets at a specific time and w_∞ is the weight of the pellets if all oxygen bound to iron was removed. When calculating the reduction extent, the total weight of all three pellets was used. However, when examining the microstructures, see Figs. 3–8, the reduction extent was calculated using the weight of the examined pellet.

Previous studies have reported that gangue material and additives remain unreduced inside the pellet after hydrogen reduction.²¹⁾ Consequently, the weight loss is assumed to be caused by oxygen bound to the iron leaving the pellets during reduction.

Figure 2(A) shows the reduction curves for the non-isothermal reduction experiments with respect to time, while Fig. 2(B) shows the reduction curves with respect to temperature. The figure shows that the reduction rate increases with increasing heating rate. The onset of reduction is at a temperature just above 450°C. All heating rates except for 7.7°C/min reach near complete reduction before the pellets reach a temperature of 900°C.

Figure 3 presents the micrographs of the pellets isothermally reduced at 600 and 900°C to a reduction extent of 95.3% and 97.2%, respectively. The micrographs are taken at the surface (A–B) and in the center (C–F) of each pellet. The black parts inside the micrograph are pores. The larger pores between the grains originate from the pelletizing process and are called intergranular pores. On the other hand, the smaller pores inside the grains are formed dur-

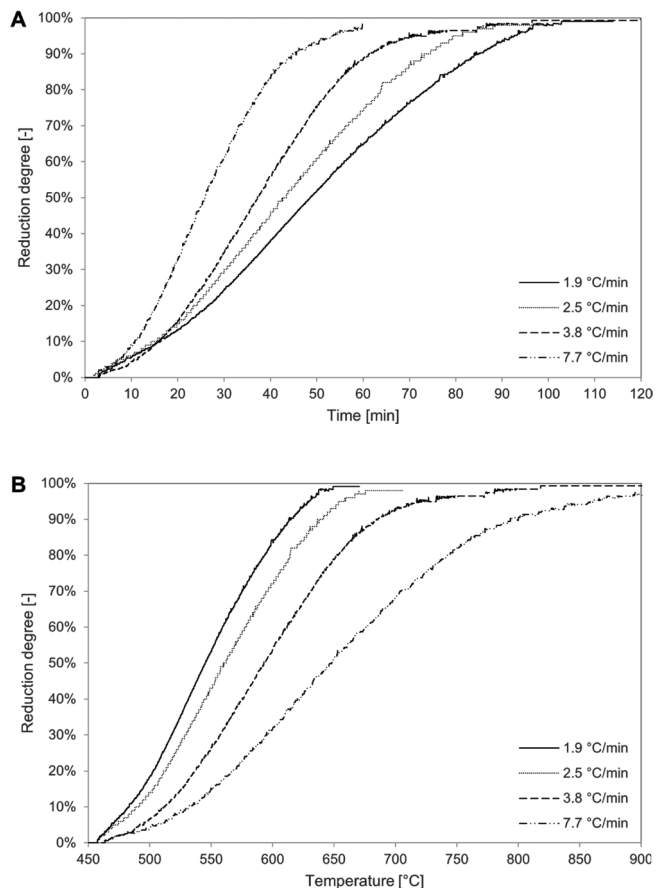


Fig. 2. Reduction curves of the non-isothermal reductions plotted against A: time and B: temperature. The non-isothermal reduction was conducted from 450 to 900°C with different heating rates: 7.7, 3.8, 2.5, and 1.9°C/min.

ing reduction and are hereinafter called intragranular pores. The size of the intragranular pores increases with increasing reduction temperature, viz., the pores formed at 600°C are

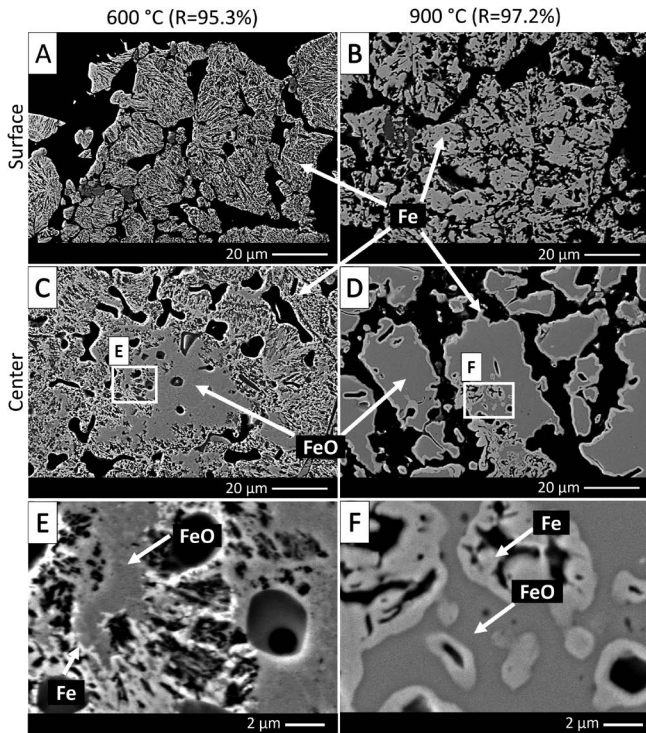


Fig. 3. Micrographs at the surface (A and B) and the center (C and D) of pellets reduced isothermally at 600 and 900°C, respectively. More magnified micrographs are shown in E and F.

smaller than the ones formed at 900°C. This is true for both the surface and the center of the pellets.

Energy dispersive spectroscopy (EDS) maps were used to analyze both pellets. The analysis showed that the grains located at the surfaces (Figs. 3(A) and 3(B)) were completely reduced and consisted of only iron. On the other hand, the grains in the center had cores containing iron oxide. The partially reduced grains, containing an iron oxide core, were surrounded by iron layers of different appearances. At 600°C, see Fig. 3(E), the iron was porous and consisted of many small intragranular pores. While at 900°C, see Fig. 3(F), the iron was dense and consisted of larger but fewer intragranular pores. In the figure, both iron and iron oxide are pointed out using arrows.

Several reduction experiments were terminated before the pellets had reached complete reduction to study the microstructure and understand how the heating rate affects the reduction. Figures 4(A)–4(I) presents the micrographs of pellets reduced to different temperatures and reduction extents using a heating rate of 7.7°C/min. From the figure, it is clear that the microstructure evolved throughout reduction. At the surface, very small intragranular pores are visible inside the grains; see Figs. 4(A)–4(C). The size and number of pores were relatively similar for the pellets reduced to 650°C or 900°C; see Figs. 4(B) and 4(C), respectively. EDS map analysis of the surface microstructure showed that the grains were completely reduced at 650°C when the total reduction extent was 49.9%.

Comparing the microstructure in the center, see Figs. 4(D)–4(I), noticeable differences were seen. In Figs. 4(D)

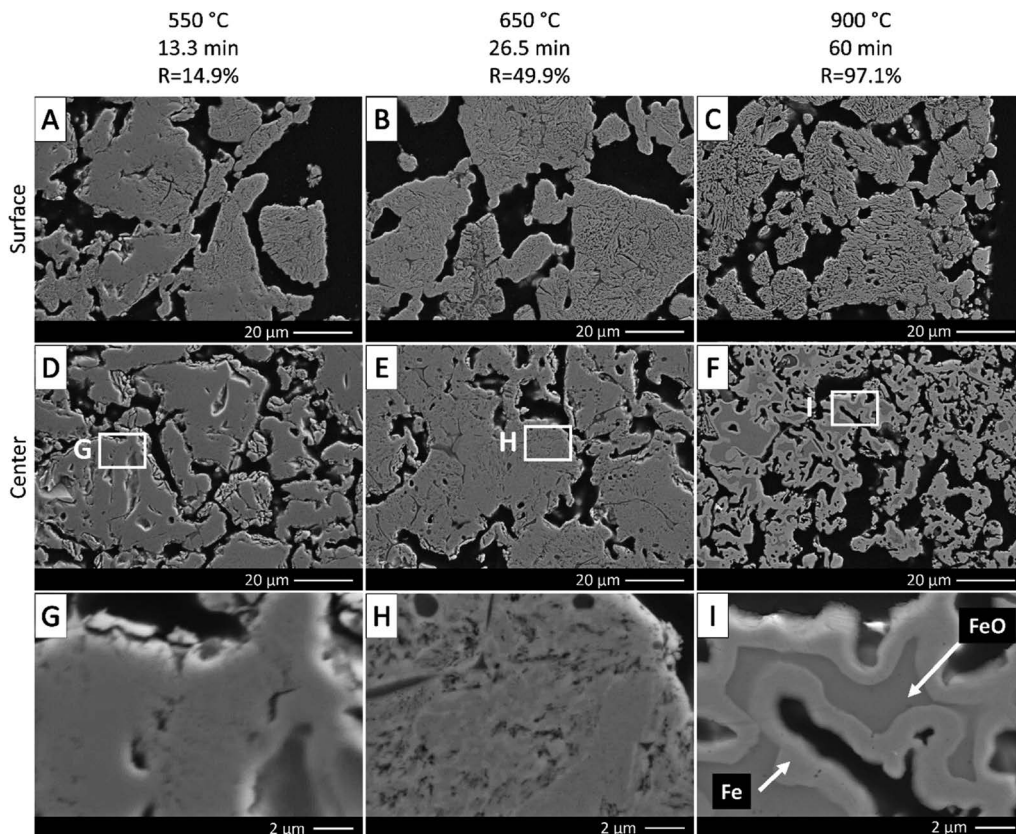


Fig. 4. Microstructures of pellets reduced using a heating rate of 7.7°C/min. The surface (A–C) and center (D–F) micrographs of pellets reduced and terminated at different reduction extents and temperatures. Higher magnification micrographs are shown in G–I.

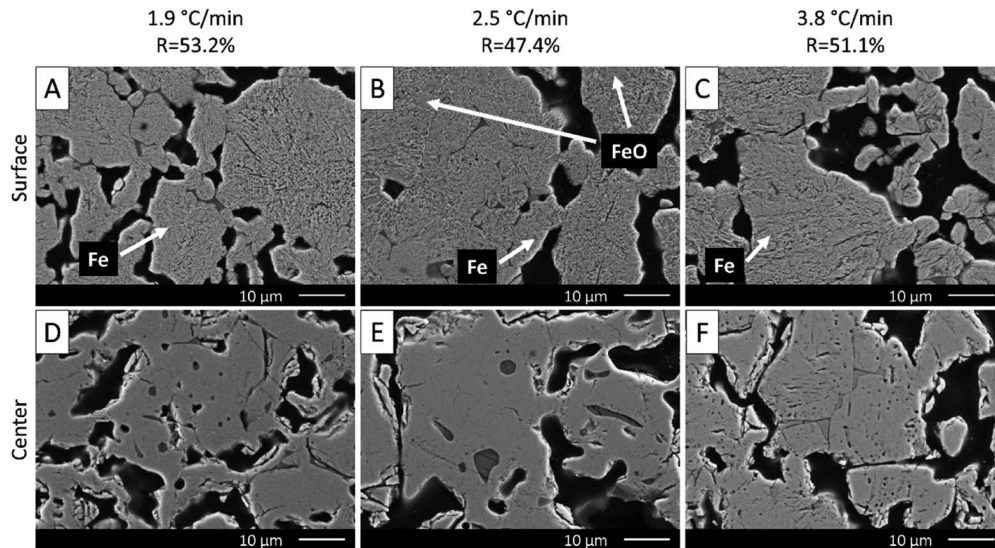


Fig. 5. Microstructures at the surface (A–C) and center (D–F) of pellets reduced using heating rates of 1.9, 2.5, and 3.8 °C/min, respectively. The reductions were terminated at a reduction extent close to 50%.

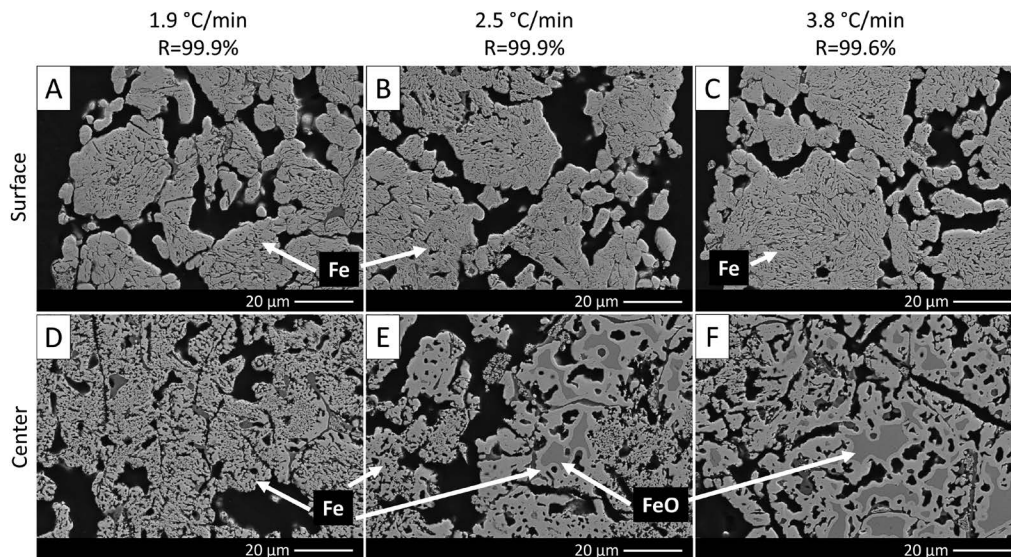


Fig. 6. Microstructures at the surface (A–C) and center (D–F) of pellets reduced using heating rates of 1.9, 2.5, and 3.8 °C/min, respectively. All reductions were terminated at a temperature of 900 °C.

and 4(G), the pellet is reduced to 14.9%, and very small and few intragranular pores were seen. As the pellets reached a reduction extent of 49.9%, the size and number of the intragranular pores increased, see Figs. 4(E) and 4(H). EDS map analysis showed that the grains contained oxygen and iron throughout. Hence, the grains in the center consist of iron oxides. Figures 4(F) and 4(I) show the center microstructure of a pellet reduced to 97.1%. As more oxygen was removed from the grains, the intragranular pore size increased, and the number of pores decreased. The EDS map analysis showed that most grains comprised iron oxide surrounded by a dense iron layer.

Figure 5 shows micrographs from pellet surface (A–C) and center (D–F) of pellets reduced to approximately 50% using heating rates 1.9, 2.5, and 3.8 °C/min. Very small but numerous intragranular pores can be seen on the surfaces. The EDS map analysis showed that no iron oxide cores could be found inside the grains located at the pellet surface, reduced using the heating rates of 1.9 and 3.8 °C/min,

see Figs. 5(A) and 5(C), respectively, only porous iron was detected. However, some iron oxide cores are found inside the grains of the pellet reduced at 2.5 °C/min, see Fig. 5(B). Both the pure iron and iron oxide were pointed out using arrows. Comparing the center microstructure, it is clear that the number of intragranular pores increased with increasing heating rate. The EDS map analysis showed that most oxygen was found in the sample reduced with the lowest heating rate, *i.e.*, 1.9 °C/min. The oxygen content gradually decreased with increasing heating rate.

Figure 6 shows the microstructure of the pellets reduced between 450 to 900 °C, to almost full extents, using different heating rates, *i.e.*, 1.9, 2.5, and 3.8 °C/min. The intragranular pores in the center (A–C) are larger than those found at the pellet's surface (D–F). Minimal differences were noted between the heating rates, *i.e.*, the grains at the surface consisted of very small intragranular pores. However, microstructural variances at the center of the pellets were noted. At the slowest heating rate, *i.e.*, 1.9 °C/min, no grains

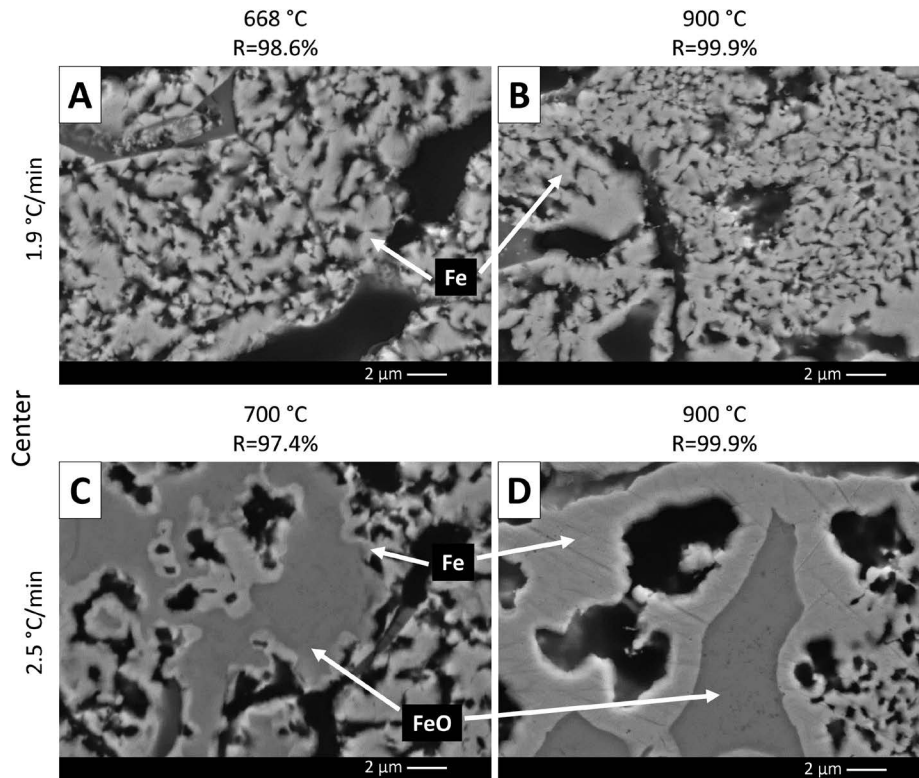


Fig. 7. Microstructures in the center of pellets terminated at different temperatures and reduced to high reduction extents using the heating rates 1.9 (A and B) and 2.5°C/min (C and D), respectively.

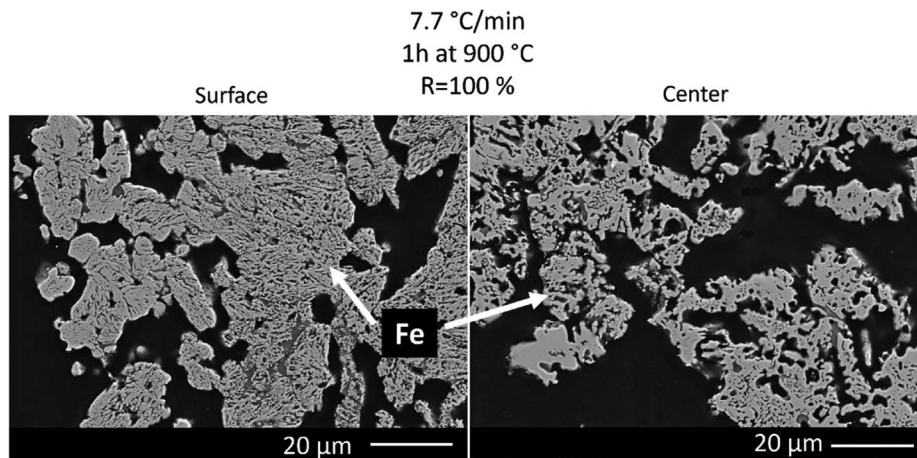


Fig. 8. Microstructure at the surface and center of pellets reduced and subsequently heated at 900°C for one hour. A heating rate of 7.7°C/min was applied.

composed of iron oxide cores surrounded by iron layers could be found; see Fig. 6(D). Instead, the grains consisted of porous iron with intragranular pores of similar sizes. In contrast, for the heating rates 2.5 and 3.8°C/min, Figs. 6(E) and 6(F) respectively, porous iron grains and iron oxide grains surrounded by a dense iron layer were found. The number of iron oxide-containing grains surrounded by an iron layer increased with increasing heating rates.

To further understand how these two different microstructures, *i.e.*, porous and dense iron, form and evolve during the late part of reduction, Figs. 7(A)–7(D) includes the micrographs at the center of the pellets reduced to different reduction extents using the heating rates 1.9 and 2.5°C/min. The intragranular pores were small and numerous inside the pellets reduced using the lowest heating rate, and no

noticeable difference was seen between the pellets reduced until 98.6% (668°C) and 99.9% (900°C), see Figs. 7(A) and 7(B), respectively. However, as shown in Figs. 7(C) and 7(D), the pellets reduced using a heating rate of 2.5°C/min showed an iron layer surrounding the iron oxide core that grew with increasing reduction extent. Additionally, grains with porous iron could be seen next to the grains with dense iron layers.

Lastly, one reduction experiment was conducted to examine the effect of sintering and prolonged time at an elevated temperature. A 7.7°C/min heating rate was applied, and the pellet was kept in the reducing atmosphere at 900°C for one hour after the non-isothermal reduction. Both the surface and center microstructures of the completely reduced pellet, *i.e.*, R=100%, are shown in Fig. 8. The intragranular pores

were larger in the center of the pellet than at the surface. No grains containing iron oxide were observed in the center.

4. Discussion

Comparing the reduction curves in Fig. 2(A), it is clear that the heating rate greatly affects the reduction rate. All reductions were initiated at 450°C, but depending on the heating rate the temperature after a certain amount of time would be different. The faster reduction rate seen for the faster heating rates, especially 7.7°C/min, can be explained by the fact that the faster heating rate experiments reach a higher reduction temperature faster than the lower heating rates. A higher reduction temperature has, by many authors, been recognized with a faster reduction rate.^{3–7} The rate sharply decreases for all experiments as the pellets approach the final percent of reduction. Shown in Fig. 2(B), the pellets reduced with the lower heating rates reach a high reduction extent at lower temperatures because they spend longer time at each temperature.

Isothermal reduction experiments were conducted at 600 and 900°C to help the discussion regarding the effect of temperature on the microstructure. Micrographs at the surface and in the center of both pellets are shown in Figs. 3(A)–3(F). The reduction temperature had a significant effect on the microstructure. The pellet reduced at the lower temperature contained grains with smaller-sized intragranular pores. These pores resulted in the formation of porous iron surrounding the remaining iron oxide cores located in the center of the pellet. The formation of smaller pores at lower temperatures confirms the result reported by Korobeinikov *et al.* and Turkdogan *et al.*^{22,23} At the higher temperature, on the other hand, larger intragranular pores were formed, and a dense iron layer surrounded the iron oxide grains found in the center. This follows the literature, where reduction at higher temperatures, resulting in a faster reduction rate, creates a microstructure with dense iron layers around the iron oxide cores.^{9–11,24}

Since the temperature significantly affected the microstructure for the non-isothermal reduction experiments, several experiments were terminated at different reduction extents to study the microstructure evolution depending on different heating rates. Shown in Figs. 4(A)–4(I), the microstructure evolved throughout reduction. In addition, and in contrast to the isothermal experiment, different microstructures were seen at the pellet's surface and center. This was previously reported by Wright.¹² At the surface of the highly reduced pellets, essentially identical microstructures were observed irrespective of heating rate; see Figs. 4(C) and 6(A)–6(C). The grains consisted of porous iron, like the microstructure found at the surface of the isothermally reduced pellet at 600°C.

The microstructure in the center contained two types of grains: highly porous iron with small and numerous intragranular pores or a dense iron layer surrounding an iron oxide core with larger and fewer pores. The latter resembles the microstructure inside the isothermally reduced pellet at 900°C. Figure 6(A) shows that only grains with porous iron were found in the center of the highly reduced pellets reduced with a heating rate of 1.9°C/min. On the contrary, all remaining heating rates contained grains with a dense

iron layer surrounding the unreduced iron oxide core, as well as some grains consisting of porous iron, see Figs. 4(F) and 6(E) and 6(F). The microstructures of Figs. 4(E) and 7(C), *i.e.*, pellets reduced with a heating rate of 7.7°C/min until 650°C, and 2.5°C/min until 700°C, was compared. Since no iron layer was found at 650°C but was clearly seen at 700°C, it is suggested that the iron layer forms between the two temperatures. Furthermore, as only porous iron is found inside the highly reduced pellet terminated at 668°C, see Fig. 7(A), it is suggested that the dense iron layer forms around the unreduced iron oxide grains at a temperature greater than 668°C. This result was in accordance with what was reported by Li *et al.*, where the solid iron layer was found to be formed at 670°C.¹⁰ A semi-quantitative analysis of the center microstructures at magnification x500 for all heating rates at high reduction extent showed that the number of grains surrounded by a dense iron layer increased with increasing heating rate. The number is shown in **Table 2** and correlated with the residual reduction extent for each heating rate above a temperature of 668°C, also seen in Table 2. As previously mentioned, adjacent to the grains with dense iron layers, grains with porous iron were found in the center of the pellets reduced at the higher heating rates. The number of grains with porous iron increased with decreasing heating rate. Accordingly, the amount of porous iron versus dense iron depends on the heating rate.

As mentioned above, the microstructural evolution was studied by terminating the reduction at different reduction extents. Figures 4(B) and 4(C), and 8(A) shows the surface microstructure of pellets reduced using a 7.7°C/min heating rate to different reduction extents, *i.e.*, 49.9%, 97.1%, and 100%, respectively. The figures show that the size and number of intragranular pores remain relatively constant even after subsequent heating, *i.e.*, between 650 to 900°C (33 min) and at 900°C for one hour. As the microstructure does not change after complete reduction, the sintering effect on the fully reduced grains under these conditions is insignificant. This contradicts what was reported by Wright, as they observed that the small pores at the surface coalesced when applying a higher temperature. However, it should be mentioned that Wright used laboratory-made pellets and a reducing gas mixture consisting of H₂–CO–CO₂ between the temperatures 450 to 950°C.¹² Lastly, because all non-isothermal reduction experiments started at a temperature of 450°C, and similar appearances at the surface were seen, it is clear that the microstructure depends on under which conditions the grains are reduced, *i.e.*, the appearance is inherited.

Understanding the microstructural evolution in the center of the pellets is also done by terminating experiments at

Table 2. Number of grains surrounded by a dense iron layer and residual reduction extent at 668°C.

Heating rate:	1.9°C/min	2.5°C/min	3.8°C/min	7.7°C/min
No. of grains surrounded by a dense iron layer	0	55	189	427
$P_{resid.}^{668^\circ\text{C}}$	0.9%	2.8%	14.7%	42.3%

different reduction extents. For the two lowest heating rates, *i.e.*, 1.9 and 2.5°C/min, the highly magnified microscope pictures displayed in Figs. 7(A)–7(D) show no noticeable coalescence of the porous iron found in the center of the pellets. However, the dense iron layer's thickness around the centermost grains reduced using a heating rate of 2.5°C/min, see Fig. 7(C) and 7(D), increased as the pellets were subsequently heated from 700°C to 900°C. The thickness grew from 0.14–0.8 μm to 0.8–2.08 μm between the temperatures 700°C to 900°C (80 min). The iron layer growth is also visible when comparing the center microstructure in Figs. 4(F) and 8(B), the layer grew from 0.74–1.46 μm to 3.76–4.71 μm when the pellet was subsequently heated at 900°C for one hour. As expected, the growth rate of the iron layer increased with increasing temperature.

To discuss the reduction of iron oxide samples using hydrogen gas in a semi-quantitative way, the reaction rate is here described using four different reduction mechanisms, *viz* (1) mass transfer in the gas phase, (2) mass transfer through the product layer, (3) chemical reaction at the product/iron oxide interface and (4) heat transfer. Because a gas flow rate of 4 nL/min hydrogen was applied for all reductions, the mechanism (1) mass transfer in the gas phase was never controlling, as a previous study in this research group had shown that this flow was above the gas starvation point.²⁰⁾

To further discuss the reduction mechanisms, Fig. 2(A) is used to analyze the reduction curves, focusing on what happens to the reaction rates above 668°C. For 7.7°C/min, the pellets reached a reduction extent of 57.7%, and a subtle but slight decrease in the overall reaction rate can be seen as the reduction continues. However, the reaction rate change was more noticeable for the 3.8°C/min heating rate. It occurred as a rather sharp decrease as the temperature increased above 668°C, where the reduction extent was 85.3%. The pellets reduced with the two lowest heating rates, 1.9 and 2.5°C/min, had reached reduction extents near complete reduction, so evaluating the reaction rate at this temperature was unnecessary. One might expect that the pellet containing the greatest number of grains surrounded by dense iron, *i.e.*, 7.7°C/min, would have the most noticeable reaction rate decrease. The dense iron layer formed at a temperature above 668°C affects the reduction mechanism (2), mass transfer in the product layer, by significantly decreasing the gas diffusion rate, agreeing with previously published data.¹⁰⁾ However, a more significant rate change was noted for the pellets reduced using the heating rate of 3.8°C/min. One possible reason could be the spread of the reaction zone, which is defined as the distance from the surface to the interface at which the reduction extent is greater than zero. Comparing the center microstructures at a reduction extent close to 50%, see Figs. 4(E) and 5(D)–5(F), it is clear that the heating rate significantly affects the reaction zone. The reaction appears to take place deeper inside the pellet as the heating rate increases since more intragranular pores are visible. Hessling *et al.* reported similar findings when comparing the reaction zone inside pellets reduced isothermally in pure hydrogen at 600 and 900°C. They suggested that the porous iron facilitates intragranular diffusion, which further reduces the grains closer to the surface, keeping the reaction zone relatively narrow.²⁴⁾ With an increasing reaction zone,

however, the mass transfer rate through the product layer is decreasing because the H₂/H₂O gas has a longer distance to diffuse. However, most likely for the case of 7.7°C/min, the overall reaction rate is limited by both the (2) mass transfer through the product layer and (3) chemical reaction at the product/iron oxide interface, already at a reduction extent of 50%. This is true as only a small rate change was noted for the 7.7°C/min heating rate as the reduction proceeded, *i.e.*, at the same time as the dense iron layer started to form at a temperature above 668°C. However, the significant rate change in the case of 3.8°C/min at a temperature above 668°C indicates that the (2) mass transfer in the gas phase also becomes limiting. Additionally, as previously mentioned, the growth rate of the formed iron layer was faster at higher temperatures, further aiding the reaction rate at the faster heating rate.

As the non-isothermal reduction experiments have shown that the microstructure evolves with reduction, it is reasonable to assume that the rate of internal mass transfer, *i.e.*, the diffusion rate, will vary with time and depend on the thermal history of the reduced sample. Similarly, the (4) heat transfer inside the sample will also vary with time, depending on the porosity and iron/iron oxide content. Consequently, an effective diffusivity and thermal conductivity that varies with both time and temperature is necessary to effectively simulate and model the non-isothermal reduction of iron oxide pellets.

Additionally, from this study, it is clear that the microstructures of isothermal and non-isothermal reduction experiments are vastly different and taking this into account when modeling the shaft furnace operation is essential; thus, failing to do so could lead to the wrong conclusions. The present study has shown the importance of increasing the understanding of non-isothermal conditions. However, inside a large-scale reactor, water will be generated as a result of the reducing reaction, which will inevitably affect the rate of reduction. Therefore, further studies on the non-isothermal reduction should consider different H₂/H₂O ratios as the water will vary with the position inside the shaft furnace due to accumulation. Studying these conditions is necessary to better understand the progression of reduction and its optimization capability. Lastly, analysis of different physical properties, *e.g.*, mechanical and aging properties of pellets after reduction using different heating rates, is vital for further realizing the direct reduction process and its optimizations.

5. Conclusion

The effect of heating rate on the non-isothermal reduction of commercial iron ore pellets using pure hydrogen gas was investigated. The experiments were performed in a resistance-heated furnace between 450 and 900°C. The applied heating rates varied between 1.9 and 7.7°C/min, and the hydrogen flow rate was selected to lay above the gas starvation flow rate. The main findings from this study are as follows: (1) Results showed that the onset temperature of iron oxide reduction using pure H₂ is close to 450°C. (2) The heating rate and method of reduction influence the microstructure. Additionally, the microstructure evolves throughout reduction. (3) The produced iron had

two different appearances depending on the temperature at which it was formed. Porous iron was formed below a temperature of 668°C while dense iron was formed above a temperature of 668°C. The amount of porous iron decreased with increasing heating rate. (4) The reaction rate sharply decreased at the iron layer formation temperature for the pellet reduced using the heating rate 3.8°C/min, due to the reduction mechanism change, *i.e.*, where the mass transfer through the iron product layer becomes limiting. However, only a small rate change was noted for the pellet reduced using the heating rate 7.7°C/min. This was due to two main reasons, one being that the reaction zone is broader at lower reduction extents, thus the reduction mechanism of mass transfer is already affecting the rate at R=50%, and secondly, the growth rate of the dense iron layer increased with increasing heating rate, aiding the overall reaction rate. (5) The porous microstructure formed at the surface at low temperatures showed no signs of coalescence even when prolonged heating was applied. The microstructure inherits its appearance depending on the reduction temperature. (6) Both the pellet conductivity and diffusion inside the pellet will change over time. Considering the time-dependent effective thermal conductivity and diffusivity is necessary when modeling the reduction inside a shaft furnace reactor.

Statement for Conflict of Interest

The authors declare that they have no conflict of interest.

Acknowledgment

The authors gratefully acknowledge the financial support of this research by Hybrit Development AB. HYBRIT (Hydrogen Breakthrough Ironmaking Technology) is a joint initiative of the three companies SSAB, LKAB, and Vattenfall, with the aim of developing the world's first fossil-free ore-based steelmaking route. The authors would also like to thank Professor Pär Jönsson for making this work possible, and Professor Emeritus Du Sichen for the support and valuable discussions.

REFERENCES

- 1) R.R. Wang, Y.Q. Zhao, A. Babich, D. Senk and X.Y. Fan: *J. Clean. Prod.*, **329** (2021), 129797. <https://doi.org/10.1016/j.jclepro.2021.129797>
- 2) O. Hessling, J.B. Fogelström, N. Kojola and D. Sichen: *Metall. Mater. Trans. B*, **53** (2022), 1258. <https://doi.org/10.1007/s11663-021-02405-1>
- 3) M. Kazemi, B. Glaser and D. Sichen: *Steel Res. Int.*, **85** (2014), 718. <https://doi.org/10.1002/srin.201300197>
- 4) E.T. Turkdogan and J.V. Vinters: *Metall. Mater. Trans. B*, **2** (1971), 3175. <https://doi.org/10.1007/BF02814970>
- 5) A. Pineau, N. Kanari and I. Gahallah: *Thermochim. Acta*, **447** (2006), 89. <https://doi.org/10.1016/j.tca.2005.10.004>
- 6) A. Ranzani da Costa, D. Wagner and F. Patisson: *J. Clean. Prod.*, **46** (2013), 27. <https://doi.org/10.1016/j.jclepro.2012.07.045>
- 7) E. Kawasaki, J. Sanscrainte and T.J. Walsh: *AIChE J.*, **8** (1962), 48. <https://doi.org/10.1002/aic.690080114>
- 8) R.J. Fruehan, Y. Li, L. Brabie and E.-J. Kim: *Scand. J. Metall.*, **34** (2005), 205. <https://doi.org/10.1111/j.1600-0692.2005.00722>
- 9) P.C. Hayes: *Steel Res. Int.*, **82** (2011), 480. <https://doi.org/10.1002/srin.201100032>
- 10) Y. Li, P. Li, J. Yu, Y. Han and P. Gao: *Steel Res. Int.*, **93** (2022), 2100749. <https://doi.org/10.1002/srin.202100749>
- 11) F. Patisson, O. Mirgoux and J.-P. Birat: *Matériaux & Techniques.*, **109** (2021), 303. <https://doi.org/10.1051/mattech/2021025>
- 12) J.K. Wright: *Trans. Iron Steel Inst. Jpn.*, **12** (1977), 726. <https://doi.org/10.2355/isijinternational1966.17.726>
- 13) M. Shimokawabe, R. Furuichi and T. Ishii: *Thermochim. Acta*, **28** (1979), 287. [https://doi.org/10.1016/0040-6031\(79\)85133-3](https://doi.org/10.1016/0040-6031(79)85133-3)
- 14) N. Towhidi: *Arch. Eisenhüttenwes.*, **55** (1984), 91. <https://doi.org/10.1002/srin.198405316>
- 15) A. Hammam, Y. Li, H. Nie, L. Zan, W. Ding, Y. Ge, M. Li, M. Omran and Y. Yu: *Min. Metall. Explor.*, **38** (2021), 81. <https://doi.org/10.1007/s42461-020-00317-3>
- 16) Z. Li, Z. Qi, L. Zhang, M. Guo, D. Liang and Q. Dong: *J. Clean. Prod.*, **409** (2023), 137059. <https://doi.org/10.1016/j.jclepro.2023.137059>
- 17) Z. Qiu, Q. Yue, T. Yan, Q. Wang, J. Sun, Y. Yuan, Z. Che, Y. Wang and T. Du: *Energy*, **263** (2023), 125847. <https://doi.org/10.1016/j.energy.2022.125847>
- 18) F. Patisson and O. Mirgoux: *Metals*, **10** (2020), 922. <https://doi.org/10.3390/met10070922>
- 19) LKAB: LKAB Product Booklet, Sweden, (2021), 21.
- 20) J.B. Fogelström, J. Martinsson and N. Kojola: *Steel Res. Int.*, **95** (2024), 2300655. <https://doi.org/10.1002/srin.202300655>
- 21) A. Vickerfält, J. Huss, J. Martinsson and D. Sichen: *Metall. Mater. Trans. B*, **54** (2023), 2206. <https://doi.org/10.1007/s11663-023-02827-z>
- 22) Y. Korobeinikov, A. Meshram, C. Harris, O. Kovtun, J. Govro, R.J. O'Malley, O. Volkova and S. Sridhar: *Steel Res. Int.*, **94** (2023), 2300066. <https://doi.org/10.1002/srin.202300066>
- 23) E.T. Turkdogan, R.G. Olsson and J.V. Vinters: *Metall. Mater. Trans. B*, **2** (1971), 3189. <https://doi.org/10.1007/BF02814971>
- 24) O. Hessling, J.B. Fogelström, N. Kojola and J. Martinsson: *ISIJ Int.*, **64** (2024), 1493. <https://doi.org/10.2355/isijinternational.ISIJINT-2023-443>